RNA Tertiary Folding Monitored by Fluorescence of Covalently Attached Pyrene†

Scott K. Silverman* and Thomas R. Cech*

Howard Hughes Medical Institute and Department of Chemistry and Biochemistry, University of Colorado at Boulder, Boulder, Colorado 80309-0215

Received June 10, 1999; Revised Manuscript Received September 3, 1999

ABSTRACT: The pathways by which large RNAs adopt tertiary structure are just beginning to be explored, and new methods that reveal RNA folding are highly desirable. Here we report an assay for RNA tertiary folding in which the fluorescence of a covalently incorporated chromophore is monitored. Folding of the 160-nucleotide *Tetrahymena* group I intron P4−P6 domain was used as a test system. Guided by the P4−P6 X-ray crystal structure, we chose a nucleotide (U107) for which derivatization at the 2′-position should not perturb the folded conformation. A 15-mer RNA oligonucleotide with a 2′-amino substitution at U107 was derivatized with a pyrene chromophore on a variable-length tether, and then ligated to the remainder of P4−P6, providing a site-specifically pyrene-labeled P4−P6 derivative. Upon titration of the pyrene-derivatized P4−P6 with Mg^{2+}, the equilibrium fluorescence intensity reversibly increased several-fold, as expected if the probe's chemical microenvironment changes as the RNA to which it is attached folds. The concentration and specificity of divalent ions required to induce the fluorescence change ($Mg^{2+} \approx Ca^{2+} > Sr^{2+}$) correlated well with biochemical folding assays that involve nondenaturing gel electrophoresis. Furthermore, mutations in P4−P6 remote from the chromophore that shifted the Mg^{2+} folding requirement on nondenaturing gels also affected in a predictable way the Mg^{2+} requirement for the fluorescence increase. Initial stopped-flow studies with millisecond time resolution suggest that this fluorescence method will be useful for following the kinetics of P4−P6 tertiary folding. We conclude that a single site-specifically tethered chromophore can report the formation of global structure of a large RNA molecule, allowing one to monitor both the equilibrium progress and the real-time kinetics of RNA tertiary folding.

As more high-resolution RNA structures become available, greater attention is being devoted to determining the pathways by which large RNAs adopt tertiary structure. Available methods for following the kinetics of RNA tertiary folding include chemical modification (*1*), oligonucleotide hybridization (*2*−*4*), ultraviolet cross-linking (*5*), and synchrotron hydroxyl radical footprinting (*6*). The first three types of experiment can provide information only on the 10 s or slower time scale. The newly described synchrotron hydroxyl radical footprinting method (*6*) is capable of resolving 20 ms folding events and has exquisite spatial resolution, monitoring the accessibility of each nucleotide separately. On the other hand, it has an inherently low signal-to-noise ratio and requires access to a synchrotron.

Fluorescence assays have many advantages for monitoring protein or RNA folding events. A chromophore's fluorescence intensity or emission spectrum, or both, may be extremely sensitive to chemical microenvironment. As a biomolecule folds, a covalently attached or noncovalently associated chromophore is typically exposed to a different microenvironment, altering its fluorescence properties. Because these properties respond extremely rapidly to environmental changes, folding events may be monitored on the millisecond or faster time scale. For RNA, fluorescence can provide at least 1 order of magnitude more time resolution than is available with the other analytical methods described above [comparable time resolution has been reported for RNA folding and unfolding using rapid absorbance measurements (*7*−*9*)]. Additionally, fluorescence spectrometers and stopped-flow cells are readily accessible, so the technique may be used widely.

Fluorescence is often used to monitor protein folding and unfolding (*10*), by following fluorescence changes both of the natural tryptophan chromophore (*11*, *12*) and of probes either covalently attached or noncovalently associated. Several studies have also investigated RNA conformational changes with fluorescence techniques. Two-chromophore fluorescence resonance energy transfer (FRET) experiments are common (*13*, *14*), and a few time-resolved FRET experiments with RNA have been described (*15*−*17*). A number of reports involve use of only one chromophore in monitoring RNA folding (*18*). Such experiments typically involve 5′- or 3′-labeling of a short RNA oligonucleotide with a fluorescent chromophore. The labeled oligonucleotide associates bimolecularly with a larger RNA, followed by folding events that affect the observed fluorescence emission intensity (*19*−*21*). This method has been used to follow an

† This work was supported by Grant GM28039 from the National Institutes of Health. S.K.S. was supported by an American Cancer Society postdoctoral fellowship and is a fellow of the Helen Hay Whitney Foundation. T.R.C. is an Investigator of the Howard Hughes Medical Institute and an American Cancer Society Professor.

* To whom correspondence should be addressed: Department of Chemistry and Biochemistry, Campus Box 215, University of Colorado at Boulder, Boulder, CO 80309-0215. Phone: (303) 492-5607 for S.K.S. and (303) 492-8606 for T.R.C. Fax: (303) 492-6194. E-mail: Scott.Silverman@colorado.edu.

10.1021/bi991333f CCC: $18.00
Published on Web 10/07/1999

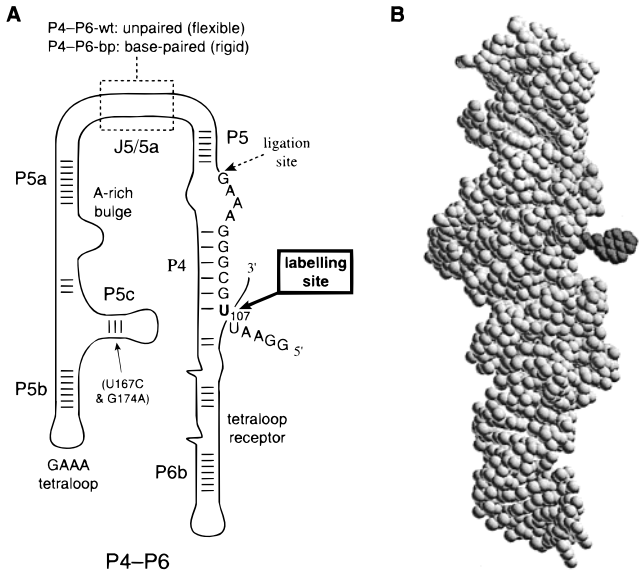

FIGURE 1: P4−P6 domain of the *Tetrahymena* group I intron RNA. (A) Secondary structure model of P4−P6. Mutation of unpaired bases in the J5/5a hinge region to form base pairs creates the P4−P6-bp mutant, which cannot undergo tertiary folding. The first 15 nucleotides of the 160-nucleotide domain are shown explicitly; these were synthesized as an oligonucleotide and ligated to a 145-nucleotide T7 transcript that comprises the remainder of P4−P6 (Δ15-P4−P6, shown as a continuous solid line). Nucleotide U107 (bold, sixth base from the 5′-end) was substituted with its 2′-amino analogue and derivatized with pyrene to form the fluorescently labeled P4−P6 RNAs used in this study. (B) A space-filling model of P4−P6 (light), with the pyr3 chromophore (dark) appended at the 2′-amino of nucleotide U107. The P4−P6 portion of the model is derived from the P4−P6 X-ray crystal structure (*27*). The molecule is shown looking directly from the right of the structure in panel A (image generated with the program O). The chromophore and tether are shown in a relatively extended conformation pointing away from the bulk of P4−P6, although the true conformation in fully folded P4−P6 is unknown.

RNA tertiary folding event (*19*). Here we describe the use of pyrene attached covalently and site-specifically to an internal 2′-amino of a large RNA, a method made possible by the availability of 2′-amino-2′-deoxynucleoside phosphoramidites (*22*−*24*). Such internal labeling offers a much wider array of possible derivatization sites, in comparison to only one 5′-end and one 3′-end per molecule. We chose pyrene over other commonly used chromophores such as fluorescein (*21*, *25*) because the fluorescence intensity of pyrene depends particularly strongly on environment when attached to nucleic acids (*26*).

As a test system for our fluorescence studies, we selected the 160-nucleotide P4−P6[1] domain of the *Tetrahymena* group I intron (Figure 1), for which a crystal structure is available (*27*). Previous work has shown that the folding of the group I intron does not depend on the direction from which the folding equilibrium is approached (*28*), and we have demonstrated this for P4−P6 itself (*29*). The unimolecular tertiary folding of P4−P6 is initiated by addition of Mg^{2+} ions. In the folded state, the P5abc subdomain nestles against the P4+P6 subdomain, resulting in a compact structure that is stabilized by several Mg^{2+} ions (*27*, *30*). When in the context of the whole ribozyme, the P4−P6 domain folds to the compact state with half-life on the order of 1 s as determined by synchrotron hydroxyl radical footprinting (*6*). The study presented here describes equilibrium fluorescence measurements with pyrene-labeled P4−P6 that validate the use of a tethered fluorescencent chromophore in tracking Mg^{2+}-induced P4−P6 tertiary folding. In addition, initial stopped-flow experiments (with ∼1 ms time resolution) suggest that this fluorescence technique will be useful in resolving the real-time kinetics of P4−P6 tertiary folding. This method may be able to be generalized to the tertiary folding of many large RNAs.

MATERIALS AND METHODS

Cloning, RNA Preparation, and Radiolabeling. Wild-type P4−P6 (denoted P4−P6-wt) was the natural sequence previously reported (*27*) encoded by a plasmid derived from the pTZL-21 construct (*31*). The J5/5a-base-paired mutant of P4−P6 (P4−P6-bp) was also as previously reported (*32*) in the pUC19 vector. Plasmid DNAs encoding P4−P6 RNAs missing the first 15 nucleotides (Δ15-P4−P6 constructs) were prepared by PCR from the P4−P6-wt or P4−P6-bp plasmids. All Δ15-P4−P6 constructs were subcloned into pUC19 and verified by automated sequencing over both ligation sites. All plasmids were linearized with *Ear*I. RNA was transcribed in vitro using T7 RNA polymerase prepared by A. Gooding in the Cech lab. Transcription conditions for full-length P4−P6 RNAs were as follows: 20 μg/mL linearized plasmid DNA, 40 mM Tris (pH 8.0), 40 mM DTT, 30 mM $MgCl_2$, each NTP at 4 mM, 2 mM spermidine, 25 °C, and 15−20 h. Transcription conditions for Δ15-P4−P6 RNAs were as follows: 20 μg/mL linearized plasmid DNA, 40 mM Tris (pH 8.0), 10 mM DTT, 10 mM $MgCl_2$, each NTP at 1 mM, 10 mM GMP, 2 mM spermidine, 37 °C, and 5 h (note that GMP was included so that the majority of the transcripts have a 5′-monophosphate as required for the splint ligations as described below). RNA was purified by PAGE, isolated, and quantified as described previously (*29*). For radiolabeling, 25−50 pmol of RNA was dephosphorylated (if required) with calf intestinal phosphatase (CIP, Boehringer), and then incubated with 25 pmol of [γ-^{32}P]ATP (6000 Ci/mmol, NEN) and 10 units of T4 polynucleotide kinase (PNK, New England Biolabs) for 10−30 min, followed by PAGE purification.

Preparation of Pyrene-Derivatized RNAs. Our strategy for preparing pyrene-derivatized P4−P6 relies on site-specific substitution of a single 2′-hydroxyl group of an oligonucleotide with a 2′-amino group, followed by reaction of the 2′-amino with a suitably activated pyrene derivative. Because the oligonucleotide bearing the 2′-amino group is only a fragment of P4−P6, the pyrene-labeled oligonucleotide must then be ligated to the remainder of P4−P6. To derivatize 2′-amino groups, we used two activated pyrene reagents, the *N*-hydroxysuccinimide (NHS) esters **pyr3-NHS** and **pyr1-NHS** (Figure 2A). Both reagents are commercially available from Molecular Probes (Eugene, OR), and Aldrich offers **pyr3-NHS**. The chromophore designations pyr1 and pyr3 were chosen because there are one and three saturated carbon atoms, respectively, in the linker between the pyrene chromophore and the carbonyl to which the 2′-amino is con-

[1] Abbreviations: P4−P6, P4−P6 domain of the *Tetrahymena* group I intron RNA; P4−P6-bp, the J5/5a-base-paired mutant of P4−P6 that is locked into a structure unable to undergo the major tertiary folding transition; PAGE, polyacrylamide gel electrophoresis; Tris, tris(hydroxymethyl)aminomethane; EDTA, ethylenediaminetetraacetic acid; TEMED, *N*,*N*,*N*′,*N*′-tetramethylethylenediamine.

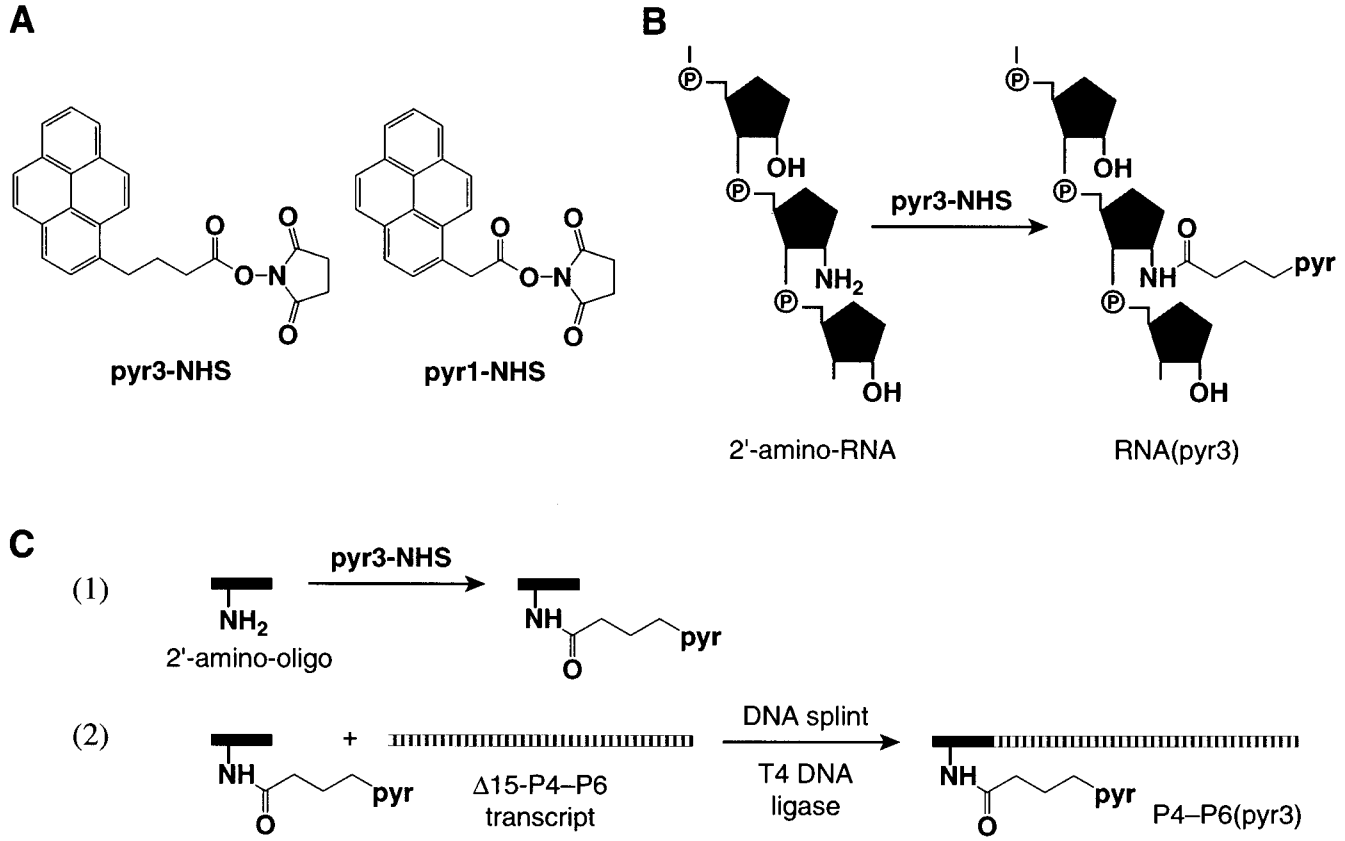

FIGURE 2: Reagents and strategies for preparing pyrene-derivatized RNA. (A) Activated pyrene derivatives **pyr3-NHS** and **pyr1-NHS**. The number after pyr represents the length in atoms of the saturated tether. (B) The reaction of **pyr3-NHS** with a generic 2′-amino-RNA to provide a pyr3-derivatized RNA, denoted RNA(pyr3). The 2′-hydroxyl groups are shown explicitly on a stylized RNA backbone (bases omitted for clarity); a single 2′-hydroxyl group is site-specifically substituted with a 2′-amino group. (C) The "derivatization then ligation" strategy for preparing pyr3-labeled P4−P6, as described in the text. Δ15-P4−P6 (striped bar) is the 145-nucleotide P4−P6 transcript missing the first 15 bases, which are provided by the modified oligonucleotide (solid bar).

nected. RNAs derivatized with these chromophores are denoted RNA(pyr3) and RNA(pyr1) (Figure 2B).

Our two-step strategy for preparing P4−P6 derivatized with either pyr3 or pyr1 at the 2′-amino of nucleotide U107 is shown in Figure 2C. In step 1, an RNA oligonucleotide comprising the first 15 nucleotides (nucleotides 102−116) of P4−P6 with a 2′-amino-U substitution at position 107 was derivatized with **pyr3-NHS** or **pyr1-NHS** and purified by 20% PAGE (the pyrene group produces a gel shift approximately equal to that caused by one additional nucleotide). The derivatization conditions were optimized using a radiolabeled oligonucleotide, as described in detail in the Supporting Information; a typical procedure is described below. In step 2, the pyrene-derivatized 15-mer was ligated with the aid of a DNA splint to a T7 transcript comprising the remaining 145 nucleotides of P4−P6 (a Δ15-P4−P6 transcript) and then purified by PAGE (see strategy 1 in ref *29*). The U107(pyr3) or U107(pyr1) group did not interfere with the ligation reaction.

*Representative Procedure for Step 1 of the Synthetic Strategy Depicted in Figure 2C: Derivatization of a 15-mer 2′-Amino Oligonucleotide with **pyr3-NHS***. To 25 nmol of 15-mer 2′-amino oligonucleotide (prepared on an Applied Biosystems synthesizer or purchased from IDT, Coralville, IA) in 120 μL of water were added 40 μL of 1 M sodium phosphate (pH 8.0), 40 μL of 1 mM EDTA, and 100 μL of DMF. To this was added 100 μL of 200 mM **pyr3-NHS** in DMF, providing 400 μL of a mixture containing 62.5 μM RNA, 50 mM **pyr3-NHS**, 100 mM sodium phosphate (pH 8.0), 0.1 mM EDTA, and 50% DMF. The cloudy white mixture was maintained at 60 °C for 4 h with occasional vortexing, and then the reaction was quenched with 1 mL of cold ethanol and the mixture kept at −20 °C for several hours. The crude product was precipitated by centrifugation at 14 000 rpm and redissolved as much as possible in 250 μL of TE (pH 8.0) and 500 μL of a solution containing 80% formamide, 1× TBE, 50 mM EDTA, 0.025% bromphenol blue, and 0.025% xylene cyanol. The product was purified by 20% PAGE as described previously (*29*), providing 4.9−6.6 nmol (20−26%) of pyr3-labeled 15-mer. The same reaction conditions gave comparable yields with **pyr1-NHS**.

Nonspecific side reactions of oligonucleotides with amino-reactive reagents have been reported (*33*). Any side reaction of the 15-mer oligonucleotide with the pyrene-NHS reagent at a site other than the desired 2′-amino will provide a product with a molecular weight equal to that of the properly derivatized oligonucleotide. On PAGE, such singly labeled side products will likely comigrate with the desired product. Therefore, we sought to demonstrate that most of the gel-purified pyrene-labeled 15-mer was derivatized at the correct site. HPLC analysis of the purified pyr3-labeled 15-mer showed that only ∼3% of the material was an unidentified product that perhaps resulted from labeling with pyr3 at a site(s) other than the 2′-amino site. An additional ∼8% of the material was the underivatized 15-mer, which cannot lead to any signals in the fluorescence experiments. We reacted

13-mers of A, C, and U as well as $(AG)_6A$ with **pyr3-NHS** to determine if one specific base is responsible for any side products (PAGE analysis; data not shown). These experiments suggested that more than one nucleotide base may be the source of any side reactivity, but further experimentation is required to determine the precise nature of any side product(s).

In a second synthetic strategy, the derivatization and ligation steps were reversed relative to those depicted in Figure 2C. First, the underivatized 2′-amino-substituted oligonucleotide was ligated to Δ15-P4−P6, and then the full-length 160-nucleotide construct was derivatized under the same conditions used for the 15-mer in the first strategy. However, we determined that pyrene-derivatized P4−P6 prepared using this second strategy has an unacceptable level of nonspecific pyrene labeling. In a key test, the wild-type P4−P6 transcript containing no 2′-amino group was subjected to the derivatization conditions with **pyr3-NHS** and then purified by PAGE (the gel shift due to pyr3 is negligible for a 160-mer). The product was found to be labeled with pyrene to the extent that fluorescence signals could readily be observed. Therefore, we cannot be confident that any signals from material prepared by the second, ligation−derivatization strategy are due to site-specifically incorporated pyrene. Apparently, the larger number of potentially reactive sites on a 160-nucleotide RNA versus a 15-nucleotide oligomer raises the chances of incorrect modification such that the level of nonspecific labeling is unacceptable. It is conceivable that such nonspecific labeling could prove to be useful in some circumstances. However, for the study presented, we desired site-specific labeling, so we used only the strategy depicted in Figure 2C.

Very recently, we have synthesized a uridine derivative in which pyrene is incorporated into a phosphoramidite for direct solid-phase synthesis (in collaboration with S. Scaringe at Dharmacon Research, Boulder, CO) of pyrene-labeled oligoribonucleotides (S. K. Silverman, unpublished results). This allows preparation of significantly greater quantities (hundreds of nanomoles) of site-specifically pyrene-labeled oligonucleotides that are highly pure. We examined the fluorescence of several pyrene-labeled RNAs prepared using this new phosphoramidite, and the results were indistinguishable from those shown in the figures (data not shown). In particular, because all components of the fluorescence titration curves were present for P4−P6 derivatives prepared using the new phosphoramidite, none of these components is due to pyrene labeling at unanticipated sites of RNA prepared by the strategy depicted in Figure 2C.

Fluorescence Spectroscopy. Equilibrium fluorescence measurements were performed using a SLM 48000S spectrometer. The cuvette holder was maintained at 25 °C with a recirculating water bath. In a typical titration procedure, the desired buffer was placed in a 1.4 mL cuvette (Uvonic type 9F, 10 mm light path) and the blank emission spectrum was recorded (excitation wavelength of 340 nm, excitation and emission band-pass settings of 4 and 8 nm, 1 nm resolution, and 10 averages per data point). RNA was added to a final concentration of ∼300 nM from a water stock solution; the sample was manually mixed with a Pasteur pipet for ∼1 min, and the emission spectrum was re-recorded. Subtraction of the blank emission spectrum provided the RNA-only emission spectrum (e.g., spectrum A in Figure 4). An aliquot of

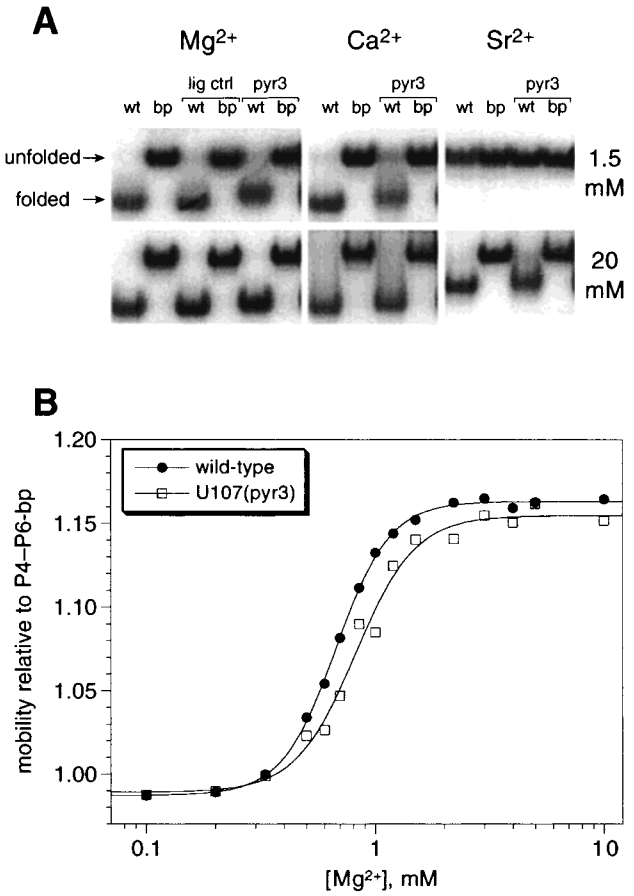

FIGURE 3: Nondenaturing gel electrophoresis of pyrene-labeled P4−P6 RNA shows that the pyrene label does not significantly disrupt folding. (A) Nondenaturing gel electrophoresis of the wild-type (wt) and unfolded control (bp) P4−P6 RNAs in 1× TB [89 mM Tris and 89 mM boric acid (pH 8)] at 35 °C with either Mg^{2+}, Ca^{2+}, or Sr^{2+}. Lanes not additionally marked contained full-length T7 transcripts of P4−P6-wt and P4−P6-bp not labeled with pyrene. The lanes labeled "lig ctrl" in addition contained ligation controls in which unlabeled P4−P6-wt was prepared by ligation of an unmodified oligonucleotide (no 2′-amino substitution) to Δ15-P4−P6 according to the strategy described in the legend of Figure 2. The lanes marked "pyr3" in addition contained the pyr3-labeled RNAs P4−P6-wt-U107(pyr3) and P4−P6-bp-U107(pyr3). Note that Mg^{2+} and Ca^{2+} promote P4−P6 folding to approximately equivalent extents, while Sr^{2+} starts to induce folding only at a much higher concentration. (B) Dependence of gel mobility on Mg^{2+} concentration. The mobility of each P4−P6 derivative relative to that of the unfolded control P4−P6-bp at various Mg^{2+} concentrations was measured, and the data were fit as described previously (*29*). The $[Mg^{2+}]_{1/2}$ values for P4−P6-wt and P4−P6-wt-U107(pyr3) determined with the same set of gels were 0.65 and 0.81 mM, respectively (the P4−P6-wt $[Mg^{2+}]_{1/2}$ value is the average of several determinations). The fit value of the Mg^{2+} Hill coefficient for the pyr3 derivative (3.3 for the data shown) was approximately the same as for P4−P6-wt (3.7 for the data shown). As described in Materials and Methods, the $[Mg^{2+}]_{1/2}$ values provide an estimate for the tertiary folding $\Delta\Delta G°'$ due to the U107(pyr3) group of 0.5 kcal/mol.

stock solution (100 mM or 1 M $MgCl_2$, $CaCl_2$, $SrCl_2$, or NaCl, or 0.5 M EDTA at pH 8.0, all in water) was added; the sample was manually mixed, and the emission spectrum was re-recorded. Because P4−P6 folding occurs on the ∼1 s time scale (*6*), the ∼1 min mixing time was sufficient to ensure complete folding after every aliquot was added. Subtraction of the blank emission spectrum and multiplicative correction for dilution relative to the RNA-only sample provided the corrected emission spectra (e.g., spectra B−D

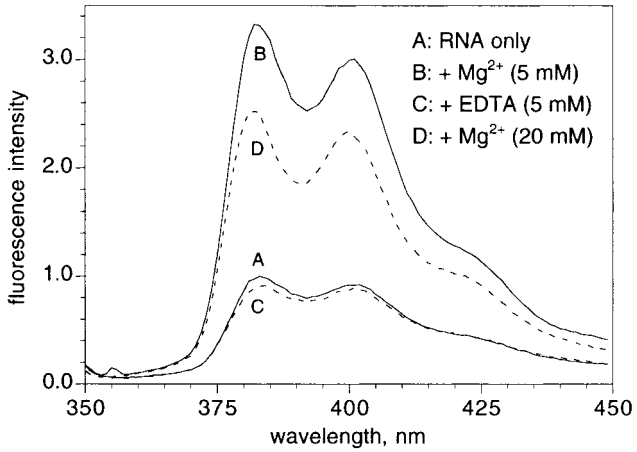

FIGURE 4: Fluorescence intensity changes for pyrene-labeled P4−P6 are due to reversible events. The fluorescence emission spectrum of a sample of 300 nM P4−P6-wt-U107(pyr3) in 10 mM Tris at pH 8.0 and 25 °C was recorded (A) as is, (B) after addition of Mg^{2+} to a final concentration of 5 mM, (C) after subsequent addition of EDTA to a final concentration of 5 mM ([Mg^{2+}] remained ∼5 mM, so free [Mg^{2+}] ≈ 0), and (D) after further addition of Mg^{2+} to a final concentration of 20 mM ([EDTA] ≈ 10 mM, so free [Mg^{2+}] ≈ 10 mM). Not shown is a spectrum recorded between C and D for which more EDTA was added to a final concentration of 10 mM (free [Mg^{2+}] ≈ 0); the spectrum was almost identical to spectrum C. The spectrum of a 10 mM Tris blank was subtracted from each spectrum before multiplicative correction for dilution, as described in Materials and Methods. The fluorescence emission λ_{max} differed by ≤2 nm for all spectra. The relative intensity is plotted in arbitrary units, normalized so that the peak intensity of spectrum A is 1.

in Figure 4). Corrections for dilution were <15% for final Mg^{2+} concentrations of 4−100 mM and up to ∼70% for the highest final Mg^{2+} concentration of 400 mM.

Two concerns with the fluorescence method are dilution correction and photobleaching. First, correction for dilution after addition of stock solution aliquots may introduce artifacts if the fluorescence intensity of the sample is not linear with respect to chromophore concentration (if, for example, the sample aggregates). Second, repeated acquisition of emission spectra may lead to photobleaching (excited-state chromophore reacting with dissolved oxygen) and a loss of emission intensity. The titration method of adding small aliquots of stock solutions followed by manual mixing may exacerbate photobleaching by resaturating the cuvette solution with oxygen before each emission scan. Purging the cuvette with inert gas to remove dissolved oxygen is impractical with up to 30 aliquot additions in most titration procedures. From inspection of Figures 5 and 6, the large dilution corrections do not appear to be problematic (the curves exhibit no discontinuity), and in any case, our conclusions depend primarily on data at ≤100 mM Mg^{2+}. To check for dilution and/or photobleaching artifacts, we repeatedly diluted (up to 27 times) samples of P4−P6-wt-U107(pyr3) and pyr3-labeled single- and double-stranded 15-mer with water and recorded emission spectra. Even with final dilution corrections of up to 71%, the maximum change in fluorescence intensity was always ≤10%, showing that combined artifacts from dilution correction and photobleaching are negligible compared with the several-fold changes in fluorescence intensity due to addition of divalent ions. In several cases, we reacquired an emission spectrum after adding the final aliquot of stock solution and exposing the

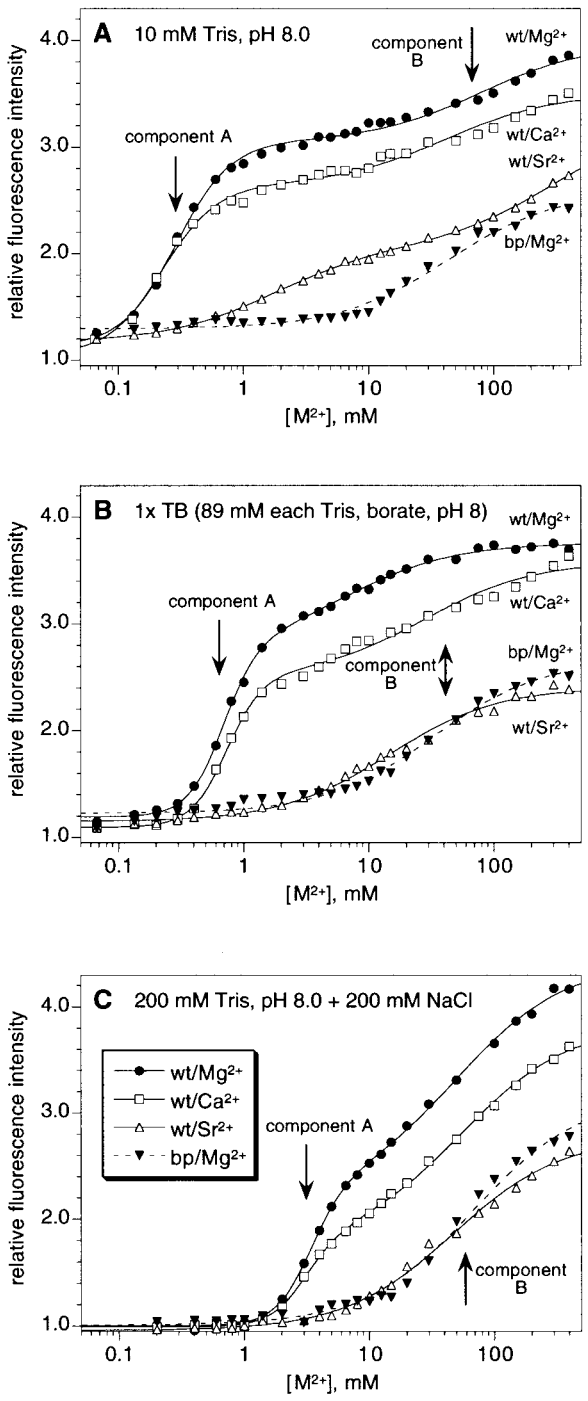

FIGURE 5: Equilibrium fluorescence titration of pyrene-labeled P4−P6 in different buffers with various divalent ions. Shown are titrations at 25 °C of P4−P6-wt-U107(pyr3) with Mg^{2+} (●), Ca^{2+} (□), and Sr^{2+} (△) and of P4−P6-bp-U107(pyr3) with Mg^{2+} (▼): (A) 10 mM Tris (pH 8.0), (B) 1× TB [89 mM Tris and 89 mM boric acid (pH 8)], and (C) 200 mM Tris (pH 8.0) with 200 mM NaCl. Mg^{2+} titrations of P4−P6-wt-U107(pyr3) in 10 mM Tris with 200 mM NaCl and in 200 mM Tris were very similar to those used to derive the data depicted in panel C (see the Supporting Information). For all full-length P4−P6 RNAs, the 380 nm relative emission intensity data are plotted. The fluorescence emission λ_{max} did not vary more than 1 nm for any particular P4−P6 sample during the course of a titration. Data were fit to the model described in Materials and Methods using eq 4; curve fit parameters are listed in Table 1. Note that the fit $[M^{2+}]_{1/2}$ values for P4−P6-wt-U107-(pyr3) with Mg^{2+} and with Ca^{2+} were essentially equivalent in all three buffers (Table 1).

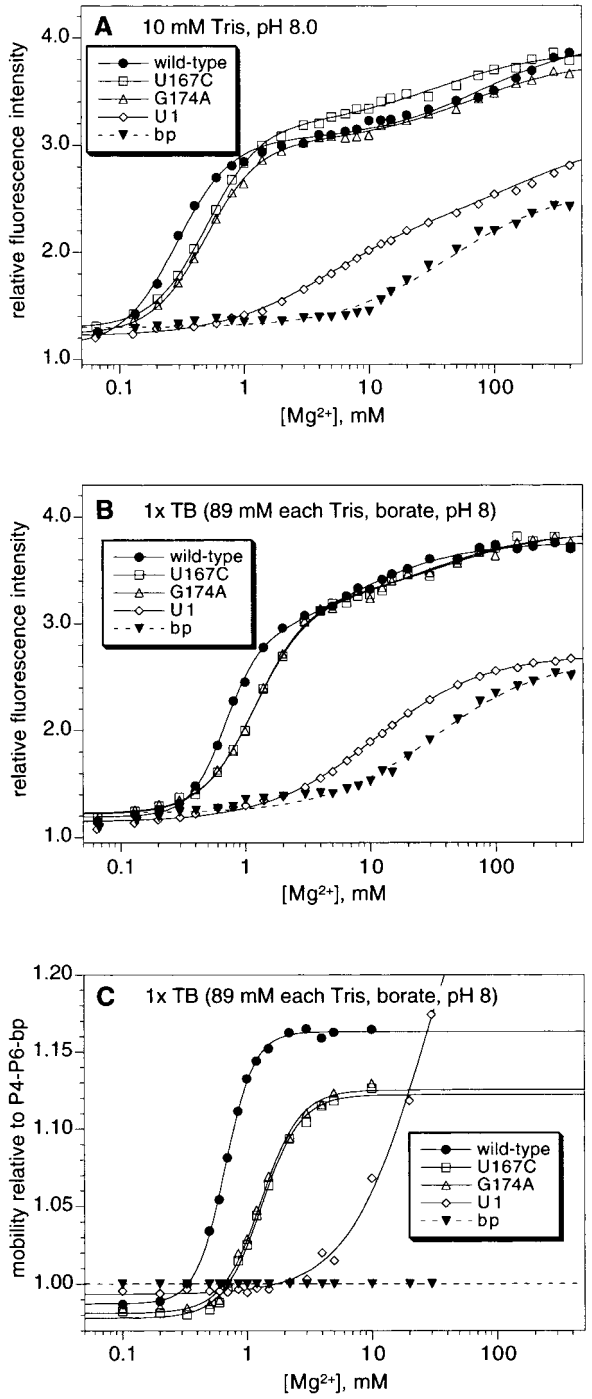

FIGURE 6: Mutations that affect P4−P6 tertiary folding also affect fluorescence titrations and nondenaturing gel mobilities. (A) Equilibrium fluorescence titrations of P4−P6-U107(pyr3) samples at 25 °C in 10 mM Tris (pH 8.0). Data were fit to eq 4; fit parameters are listed in Table 1. U167C and G174A are P5abc mutations that shift the Mg^{2+} dependence of P4−P6 folding moderately (S. K. Silverman, M. Zheng, M. Wu, I. Tinoco, Jr., and T. R. Cech, manuscript submitted for publication), while U1 is a multiple mutation in J5/5a that more strongly affects folding (*41*). (B) Analogous fluorescence titrations at 25 °C in 1× TB. (C) Nondenaturing gel mobilities at 35 °C in 1× TB for P4−P6 derivatives not labeled with pyrene. The relative gel mobility of unfolded control P4−P6-bp is defined as 1 at all Mg^{2+} concentrations. Relative mobility data were fit as described in ref *29*. $[Mg^{2+}]_{1/2}$ values and Mg^{2+} Hill coefficients n for the individual data sets shown were as follows: wild-type, 0.67 mM and 3.7; U167C, 1.31 mM and 2.8; G174A, 1.30 mM and 2.8; and U1, 27 mM and 1.4.

RNA solution to the excitation source for up to 2 h. In all such cases, the photobleaching effect was very small (≤5% in 2 h).

A simple chemical model (eq 1) was used to correlate the observed fluorescence emission intensities with ion-dependent RNA folding events.

$$\mathrm{U} \overset{n_A\ M^{2+}}{\rightleftharpoons} \mathrm{F_A} \overset{n_B\ M^{2+}}{\rightleftharpoons} \mathrm{F_B} \quad (1)$$

In the absence of divalent metal ion M^{2+}, the molecule to which the pyrene chromophore is attached is in an unfolded state U, for which the relative fluorescence intensity is defined as 1. Upon binding of n_A M^{2+} ions, the molecule adopts folded state F_A, with relative fluorescence intensity I_A. Upon binding of an additional n_B M^{2+} ions, the molecule adopts folded state F_B with relative fluorescence intensity I_B. The equilibrium constants K_A and K_B relate the concentrations of U, F_A, and F_B according to eqs 2 and 3.

$$[\mathrm{F_A}] = K_A[\mathrm{U}][M^{2+}]^{n_A} \quad (2)$$

$$[\mathrm{F_B}] = K_b[\mathrm{F_A}][M^{2+}]^{n_B} = K_AK_B[\mathrm{U}][M^{2+}]^{n_A+n_B} \quad (3)$$

In addition to all of these changes, for many titrations there is an initial component of fluorescence intensity increase at very low Mg^{2+} concentrations (e.g., see panels A and B of Figure 5). In almost every case, the change in emission intensity due to this initial component $I_{init} < 1.3$ (Table 1). The observed relative fluorescence intensity I_{obs} is then as shown in eq 4, which has up to seven independent variables (n_A, n_B, K_A, K_B, I_{init}, I_A, and I_B).

$$I_{obs} = \frac{I_{init}[\mathrm{U}] + I_A[\mathrm{F_A}] + I_B[\mathrm{F_B}]}{[\mathrm{U}] + [\mathrm{F_A}] + [\mathrm{F_B}]} = \frac{I_{init} + I_AK_A[M^{2+}]^{n_A} + I_BK_AK_B[M^{2+}]^{n_A+n_B}}{1 + K_A[M^{2+}]^{n_A} + K_AK_B[M^{2+}]^{n_A+n_B}} \quad (4)$$

To fit the equilibrium fluorescence titration data such as that depicted in Figure 5, values of n_A and n_B were fixed (e.g., $n_A = 2$ and $n_B = 1$; see Table 1), and the relative fluorescence intensity versus M^{2+} concentration data were fit (KaleidaGraph, version 3.0.2) to eq 4 with K_A, K_B, I_{init}, I_A, and I_B allowed to vary. The $[Mg^{2+}]_{1/2}$ values were calculated as $K^{-1/n}$. Errors in fit $[Mg^{2+}]_{1/2}$ values were appreciably larger when the data were fit to all seven parameters without assuming integer values of n_A and n_B. However, in these cases, the fit values of n_A and n_B were similar to the integral values used in the five-parameter fits shown in the figures. The calculated values of $[Mg^{2+}]_{1/2}$ generally changed very little when I_{init} was instead fixed at 1.0, but in many cases, the $I_{init} = 1.0$ curve fit clearly came under the first one or two low-Mg^{2+} concentration data points. For the pyrene-labeled double-stranded oligonucleotides, fixing I_{init} at 1.0 gave reasonable curve fits.

Nondenaturing (Native) Gel Electrophoresis. Gels were prepared, run, and analyzed as described previously (*29*). For thermodynamic analysis of the effect of the U107(pyr3) group on P4−P6 folding (see Figure 3), the previously described procedure was used (*29*). At 35 °C, the $[Mg^{2+}]_{1/2}$ values for P4−P6-wt and P4−P6-wt-U107(pyr3) were 0.65

Table 1: Fits of Equilibrium Fluorescence Titration Data for Pyrene-Labeled P4−P6 RNAs[a]

construct	label	ion	M^{2+} Hill coefficient(s)	component A $[M^{2+}]_{1/2}$ (mM)	component B $[M^{2+}]_{1/2}$ (mM)	intensity I_{init}	intensity I_A	intensity I_B
10 mM Tris (pH 8.0)								
wt	pyr3	Mg^{2+}	$n_A = 2$; $n_B = 1$	0.29 ± 0.01	79 ± 21	1.1	3.0	4.0
wt	pyr3	Ca^{2+}	$n_A = 2$; $n_B = 1$	0.23 ± 0.02	41 ± 11	1.1	2.6	3.5
wt	pyr3	Sr^{2+}	$n_A = 1$; $n_B = 1$	1.7 ± 0.1	320 ± 60[c]	1.2	2.1	3.3
bp	pyr3	Mg^{2+}	$n = 1$[b]	−	43 ± 4	1.3	−	2.6
U167C	pyr3	Mg^{2+}	$n_A = 2$; $n_B = 1$	0.50 ± 0.02	35 ± 7	1.3	3.2	3.9
G174A	pyr3	Mg^{2+}	$n_A = 2$; $n_B = 1$	0.49 ± 0.02	30 ± 13	1.2	3.0	3.8
U1	pyr3	Mg^{2+}	$n_A = 1$; $n_B = 1$	4.5 ± 0.6	190 ± 120	1.2	2.3	3.1
wt	pyr1	Mg^{2+}	$n_A = 2$; $n_B = 1$	0.28 ± 0.02	73 ± 8	1.4	3.7	7.3
1× TB [89 mM tris and 89 mM borate (pH 8)]								
wt	pyr3	Mg^{2+}	$n_A = 3$; $n_B = 1$	0.70 ± 0.02	12 ± 5	1.1	3.0	3.8
wt	pyr3	Ca^{2+}	$n_A = 3$; $n_B = 1$	0.73 ± 0.04	28 ± 7	1.0	2.7	3.7
wt	pyr3	Sr^{2+}	$n = 1$[b]	−	15 ± 2	1.1	−	2.4
bp	pyr3	Mg^{2+}	$n = 1$[b]	−	33 ± 4	1.2	−	2.7
U167C	pyr3	Mg^{2+}	$n_A = 2$; $n_B = 1$	1.20 ± 0.05	62 ± 10	1.2	3.2	3.9
G174A	pyr3	Mg^{2+}	$n_A = 2$; $n_B = 1$	1.22 ± 0.04	39 ± 15	1.2	3.2	3.9
U1	pyr3	Mg^{2+}	$n = 1$[b]	−	11 ± 1	1.1	−	2.7
200 mM Tris (pH 8.0) with 200 mM NaCl								
wt	pyr3	Mg^{2+}	$n_A = 3$; $n_B = 1$	3.4 ± 0.2	50 ± 5	1.0	2.2	4.4
wt	pyr3	Ca^{2+}	$n_A = 3$; $n_B = 1$	3.0 ± 0.2	55 ± 3	1.0	1.8	3.8
wt	pyr3	Sr^{2+}	$n = 1$[b]	−	47 ± 3	1.0	−	2.8
bp	pyr3	Mg^{2+}	$n = 1$[b]	−	69 ± 8	1.0	−	3.2
wt	pyr1	Mg^{2+}	$n_A = 3$; $n_B = 1$	3.3 ± 0.3	65 ± 5	1.1	2.1	6.3

[a] All P4−P6 samples were labeled with either pyr3 or pyr1 at U107 as indicated and titrated at 25 °C. The data depicted in Figures 5, 6, and 8 were fit to eq 4 of Materials and Methods with fixed values of M^{2+} Hill coefficients n_A and n_B as shown. Errors in $[M^{2+}]_{1/2}$ values are standard deviations for fitting data from individual titration experiments. In several cases, quantitatively similar fit values were obtained from repeat titrations (data not shown). Fits of component B $[M^{2+}]_{1/2}$ were not very precise, in that a wide range of values give visually acceptable fits to the data. I_{init}, I_A, and I_B represent relative fluorescence intensities during the course of an equilibrium titration as described in Materials and Methods (eq 4). Errors in the fit values of I_{init}, I_A, and I_B were <0.1 in all cases. [b] A modified form of eq 4 reflecting only one Mg^{2+}-dependent equilibrium was sufficient to fit the data. [c] With an I_{init} of 0, component B $[Mg^{2+}]_{1/2} = 160 \pm 70$ mM.

and 0.81 mM, respectively (Figure 3; the P4−P6-wt value is an average from several such experiments). The fit values of the Mg^{2+} Hill coefficients for the particular gels used to obtain Figure 3B were 3.7 and 3.3; repeated experiments with P4−P6-wt converged on a value of ~4.0 (*29*). The change in tertiary folding free energy is then calculated as $\Delta\Delta G^{\circ\prime} = 4RT \ln[[Mg^{2+}]_{1/2,wt}/[Mg^{2+}]_{1/2,U107(pyr3)}] = 0.5$ kcal/mol, where the factor 4 is the Hill coefficient. The $[Mg^{2+}]_{1/2}$ values for P4−P6-U167C, P4−P6-U167C-U107(pyr3), P4−P6-G174A, and P4−P6-G174A-U107(pyr3) were 1.31, 1.75, 1.30, and 1.80 mM, respectively (Figure 6C and data not shown). The fit values of Mg^{2+} Hill coefficients for the unlabeled and pyr3-labeled mutants were 2.8 and 2.5, respectively. Calculation of $\Delta\Delta G^{\circ\prime}$ using the wild-type Hill coefficient of 4 provided $\Delta\Delta G^{\circ\prime}$ values due to pyr3 of 0.7 and 0.8 kcal/mol in the context of the U167C and G174A mutations, respectively. A similar calculation using instead a Hill coefficient of 3 gave $\Delta\Delta G^{\circ\prime}$ values of 0.5 and 0.6 kcal/mol, respectively. All $\Delta\Delta G^{\circ\prime}$ values have estimated errors of ±0.2 kcal/mol (*29*).

RESULTS

Site-Specific Pyrene Labeling of P4−P6 RNA. An attractive strategy for site-specific fluorescent labeling of a large RNA is first to substitute a single nucleotide with its 2′-amino analogue and then to derivatize specifically the 2′-amino group with a suitably activated pyrene reagent. A similar 2′-amino labeling strategy was recently used to incorporate sulfhydryl groups into the *Tetrahymena* group I intron RNA (*34*). Because 2′-aminopyrimidine (but not purine) phosphoramidites are presently commercially available for automated oligonucleotide synthesis, we restricted ourselves to pyrimidine nucleotides of P4−P6 as candidates for 2′-labeling. We inspected the P4−P6 crystal structure (*27*), looking for sites at which to append a pyrene chromophore without disrupting the folded structure. Among the 5′-terminal nucleotides of P4−P6 (Figure 1A), the 2′-hydroxyl of U107 appeared to be positioned favorably for substitution with 2′-amino and derivatization with a relatively large pyrene chromophore (Figure 1B). Therefore, U107 was targeted for replacement with its 2′-amino analogue and derivatization with pyrene.

We followed the synthetic strategy shown in Figure 2C. A 15-mer RNA oligonucleotide corresponding to the first 15 nucleotides of P4−P6 and with a 2′-amino at U107 was labeled with pyrene using one of the commercially available *N*-hydroxysuccinimide esters, **pyr3-NHS** and **pyr1-NHS** (Figure 2A; the number after "pyr" indicates the length in atoms of the saturated tether between the pyrene moiety and the reactive carbonyl group). These reagents react reasonably well with 2′-amino groups to give the corresponding stable amides (*35*, *36*), as depicted in Figure 2B and described in Materials and Methods. The derivatized oligonucleotide was then ligated to a T7 transcript comprising the remaining 145 nucleotides of P4−P6 (Δ15-P4−P6 RNA), using a previously reported splint ligation strategy (*29*, *37*). This provides the full-length pyrene-labeled P4−P6 in a single ligation step. Minimizing the number of ligation steps is important because orders of magnitude more RNA are required for fluorescence (~1 nmol) than are used in, for example, gel studies with

radiolabeled RNAs (≥10 pmol). An alternative strategy in which the ligation and derivatization steps were switched was unsuitable because of nonspecific labeling of the RNA (see Materials and Methods). As described below, we have concentrated most of our efforts on the pyr3 derivatives of P4−P6.

Labeling P4−P6 with pyr3 at U107 Does Not Greatly Disrupt Tertiary Folding. The major Mg^{2+}-dependent tertiary folding transition in wild-type P4−P6 (P4−P6-wt) moves the P5abc subdomain next to the P4+P6 subdomain of the RNA, forming a relatively compact folded state (*27*, *38*). The P4−P6 derivative P4−P6-bp is locked into an extended conformation because the flexible J5/5a "hinge" region has been made rigid by base pairing (Figure 1A) (*32*). Therefore, P4−P6-bp serves as a control molecule that cannot undergo tertiary folding. Both P4−P6-wt and P4−P6-bp were labeled with pyr3 at U107 using the derivatization−ligation strategy depicted in Figure 2C, providing the pyrene-labeled analogues P4−P6-wt-U107(pyr3) and P4−P6-bp-U107(pyr3). Unlabeled wild-type P4−P6 exhibits a nondenaturing gel tertiary folding transition at $[Mg^{2+}]_{1/2} \approx 0.7$ mM in a standard Tris-borate buffer [1× TB being 89 mM Tris and 89 mM boric acid (pH 8); see Figure 3 and ref *29*]. We found that labeling with pyr3 at U107 does not greatly disrupt the Mg^{2+}-dependent tertiary folding of P4−P6. In particular, the folding transition of P4−P6-wt-U107(pyr3) is shifted <0.2 mM Mg^{2+} relative to that of unlabeled P4−P6-wt (Figure 3B), corresponding to a change in tertiary folding free energy ($\Delta\Delta G°'$) of only 0.5 kcal/mol as an effect of the pyrene label (see Materials and Methods). Similar results were observed with pyr1-labeled P4−P6 ($\Delta\Delta G°' = 0.5$ kcal/mol; data not shown). Substitution of the U107 2′-hydroxyl with 2′-methoxy results in no significant destabilization [$\Delta\Delta G°' = 0.1 \pm 0.2$ kcal/mol (*29*)].

Mg^{2+} Induces Reversible Changes in the Fluorescence of Pyrene-Labeled P4−P6. When Mg^{2+} was added to P4−P6-wt-U107(pyr3), the fluorescence emission intensity increased more than 3-fold (Figure 4), while the emission λ_{max} remained essentially unchanged, as expected from previous studies (*26*). We verified that the fluorescence intensity changes for pyrene-labeled P4−P6 were due to reversible events. The intensity of P4−P6-wt-U107(pyr3) fluorescence emission increased 3.5-fold upon addition of 5 mM Mg^{2+} but returned to the pre-Mg^{2+} level upon chelation of the Mg^{2+} with 5 mM EDTA. Addition of more EDTA (to 10 mM) had no further effect. Subsequent addition of excess Mg^{2+} (20 mM; ∼10 mM free Mg^{2+}) restored a 3-fold fluorescence increase (Figure 4). In contrast to the observations with Mg^{2+}, titration of P4−P6-wt-U107(pyr3) with up to 400 mM Na^+ or dilution with water caused only minor changes in fluorescence (<10% increase; see the Supporting Information). This is consistent with the expectation that Mg^{2+} induces specific tertiary folding of P4−P6, whereas Na^+ does not.

Equilibrium Titration of pyr3-Labeled P4−P6 with Mg^{2+} Reveals Several Fluorescence Components. We obtained equilibrium fluorescence Mg^{2+} titration curves for P4−P6-wt-U107(pyr3) and P4−P6-bp-U107(pyr3) in 10 mM Tris at pH 8.0 and 25 °C over nearly 4 orders of magnitude of Mg^{2+} concentrations (0.065−400 mM; Figure 5A). The Mg^{2+} titration curve for both derivatives showed an initial slight (<30%) increase in fluorescence at <0.1 mM Mg^{2+} that does not correspond to large-scale tertiary folding (see below) and is therefore likely due to local adjustment of structure. At higher Mg^{2+} concentrations, the observed fluorescence increase in the wild-type derivative fit well to a standard binding curve (eq 4) with two Mg^{2+}-dependent components. The first component, denoted A, had a $[Mg^{2+}]_{1/2}$ of 0.3 mM and was responsible for the majority of the Mg^{2+}-induced fluorescence intensity increase. The second component, denoted B, had a $[Mg^{2+}]_{1/2}$ of ≈80 mM and contributed much less than component A to the overall fluorescence intensity increase. For the P4−P6-bp derivative, which cannot undergo tertiary folding, the initial component and component B were present, but component A was clearly absent.

We chose a wider range of buffer conditions under which to examine the fluorescence changes. The Mg^{2+} titrations were repeated in the same Tris-borate buffer (1× TB) that was used for the nondenaturing gels of Figure 3 (Figure 5B). The highest-ionic strength buffer we tested was 200 mM Tris (pH 8.0) with 200 mM NaCl (Figure 5C). We also examined 10 mM Tris with 200 mM NaCl as well as 200 mM Tris (both pH 8.0), each of which gave results similar to those with the highest-ionic strength buffer (see the Supporting Information). In all the buffers that were tested, the equilibrium titration curves for P4−P6-wt-U107(pyr3) appeared to have the same two components (A and B) as in 10 mM Tris, while P4−P6-bp-U107(pyr3) again had only component B. Fluorescence component B was a relatively minor component of the P4−P6 titration curves. In the lower-ionic strength buffers, although component A led to a 3-fold emission intensity increase, component B contributed only an additional 20−40% increase. In the highest-ionic strength buffer, components A and B contributed about equally to the overall fluorescence increase. The $[Mg^{2+}]_{1/2}$ for component A was markedly buffer-sensitive (Table 1). In contrast, the $[Mg^{2+}]_{1/2}$ for component B depended less on buffer. In particular, the component B $[Mg^{2+}]_{1/2}$ was essentially the same in 10 mM Tris and in 200 mM Tris with 200 mM NaCl, while the component A $[Mg^{2+}]_{1/2}$ varied over 1 order of magnitude between the same two buffers.

Tentative Identification of Fluorescence Component A as Being Due to Tertiary Folding of P4−P6. Several lines of evidence suggested that fluorescence component A was due to P4−P6 tertiary folding. First, in all the buffers that were tested, component A was present in Mg^{2+} titrations of P4−P6-wt-U107(pyr3) but not P4−P6-bp-U107(pyr3), which cannot physically undergo tertiary folding. Second, the observed $[Mg^{2+}]_{1/2}$ for component A was as expected for the known tertiary folding of P4−P6. In particular, the $[Mg^{2+}]_{1/2}$ of 0.7 mM for fluorescence component A in 1× TB buffer (Figure 5B) was consistent with the nondenaturing gel $[Mg^{2+}]_{1/2}$ values of ∼0.7−0.8 mM for P4−P6-wt and P4−P6-wt-U107(pyr3) in the same buffer (Figure 3B). Finally, the fluorescence titration curves showed evidence of Mg^{2+} cooperativity, a known feature of P4−P6 folding (*29*, *30*). For titration data obtained in 10 mM Tris, component A was fit well with a Mg^{2+} Hill coefficient n_A of 2, while in 1× TB and in 200 mM Tris with 200 mM NaCl, acceptable fits required an n_A of ≥3. In the latter buffers, fits with an n_A of 3 or 4 differed very little visually, while fits with an n_A of 1 were extremely poor in all buffers (not shown).

We designed two general sets of experiments to test further the proposed correlation between fluorescence component A and tertiary folding. First, the divalent cation specificity of component A should agree with that of P4−P6 folding on nondenaturing gels. Second, component A should respond predictably to mutations in P4−P6 that shift the Mg^{2+} dependence of folding on nondenaturing gels.

Fluorescence Component A Responds to Different Divalent Ions As Predicted from Nondenaturing Gel Analysis of Tertiary Folding. On nondenaturing gels, P4−P6-wt folded approximately as well with Ca^{2+} as with Mg^{2+}, but only poorly with Sr^{2+}; appending the pyr3 label did not affect this specificity (Figure 3A). The fluorescence of P4−P6-wt-U107(pyr3) was monitored during titration with Ca^{2+} and Sr^{2+} as for Mg^{2+} in several buffers (Figure 5). The same trend with fluorescence as seen on the nondenaturing gels was observed; Ca^{2+} triggered component A of the fluorescence changes about as well as Mg^{2+} (Table 1), while Sr^{2+} induced a fluorescence increase only at a much higher concentration. These results are as expected if fluorescence component A is indeed due to tertiary folding of P4−P6 (*39*, *40*).

Fluorescence Component A Responds to Mutations in P4−P6 As Predicted from Nondenaturing Gel Analysis. We examined several mutations that disrupt Mg^{2+}-dependent P4−P6 folding either weakly or strongly. The mutations U167C and G174A are in the P5c stem, remote from the site of pyrene labeling (Figure 1A). In P4−P6 not labeled with pyrene, these mutations moderately disrupted tertiary folding, with a shift in $[Mg^{2+}]_{1/2}$ from 0.7 to 1.3 mM on nondenaturing gels (Figure 6C; S. K. Silverman, M. Zheng, M. Wu, I. Tinoco, Jr., and T. R. Cech, manuscript submitted for publication). Appending the pyr3 label at U107 of the mutants led to $\Delta\Delta G°'$ values (0.5−0.8 kcal/mol) that were similar to those for derivatizing wild-type P4−P6 with pyr3 (see Materials and Methods). Consistent with measurable folding disruption due to U167C and G174A, the Mg^{2+} fluorescence titrations of P4−P6-U167C-U107(pyr3) and P4−P6-G174A-U107(pyr3) (prepared by splint ligation of pyr3-labeled 15-mer and the appropriately mutated Δ15-P4−P6 transcripts) were shifted slightly relative to that of P4−P6-wt-U107(pyr3) (Figure 6A,B). We also examined the more strongly disruptive, previously reported U1 mutation that modifies the J5/5a hinge region (*41*). For the U1 mutant, on nondenaturing gels a large Mg^{2+} shift was observed, and as anticipated the pyrene-labeled mutant P4−P6-U1-U107-(pyr3) exhibited a substantial shift in the Mg^{2+} concentration dependence of its fluorescence component A. Therefore, both weakly and strongly perturbing mutations predictably shift the Mg^{2+} dependence of component A, as expected if component A reflects P4−P6 tertiary folding.

Fluorescence Changes Observed with Pyrene-Labeled Oligonucleotides Suggest That Component B Is Due to Local Reorganization, Not Tertiary Folding. In contrast to fluorescence component A, component B was not very sensitive to specific divalent ion identity (Figure 5). In addition, remote mutations that significantly affect the component A Mg^{2+} dependence shifted component B to a smaller extent (Figure 6). We therefore suspected that component B was not due to large-scale tertiary folding. If more local structural changes are responsible for component B, then similar fluorescence changes might be observed upon adding divalent ions to pyrene-labeled oligonucleotides that have no tertiary structure, to the extent that these smaller molecules are able to undergo analogous structural transitions. We thus examined fluorescence titrations of a short pyrene-labeled RNA oligonucleotide, in both single- and double-stranded forms, using the same pyr3-labeled 15-mer that was ligated to form full-length P4−P6.

The pyr3-labeled single-stranded oligonucleotide exhibited a *decrease* in fluorescence intensity upon titration with monovalent or divalent ions in 10 mM Tris (Figure 7A). The effect of Sr^{2+} was somewhat larger than that of Mg^{2+}. This contrasts with the data for full-length P4−P6, for which Sr^{2+} is significantly less effective than Mg^{2+} in inducing the fluorescence changes (Figure 5).

The pyr3-labeled double-stranded oligonucleotide was prepared by mixing the pyr3-labeled single-stranded 15-mer with its complement before titration. The absolute emission intensity of the pyrene-labeled oligonucleotide was several times higher than that of the full-length P4−P6 RNA at the same concentration and spectrometer settings (data not shown). Na^+ induced a small fluorescence increase for the double-stranded oligonucleotide only at very high concentrations (> 50 mM; Figure 7B). Titration with divalent ions led to an increase in fluorescence intensity at a concentration that depended on buffer identity, followed by an intensity decrease at very high concentrations (>100 mM; Figure 7C). Sr^{2+} had a slightly greater effect than did Mg^{2+}. This contrasts with the behavior of component A of full-length P4−P6, which was induced by Mg^{2+} much more efficiently than by Sr^{2+}, but parallels component B of P4−P6. Although the overall magnitude of the fluorescence increase observed with the pyr3-labeled oligonucleotides was comparable to that observed with labeled P4−P6 (2−4-fold), the fluorescence changes with the oligonucleotides were clearly not cooperative with respect to divalent ions. In particular, the data fit well with values for all M^{2+} Hill coefficients of 1 (Figure 7).

Examination of Annealing Effects. For some RNAs, tertiary structure can depend on the particular history of a sample because of kinetic folding traps (*42*, *43*). Although this is not the case with P4−P6 (*29*), we investigated the effect of annealing (refolding) the pyrene-labeled P4−P6 before Mg^{2+} fluorescence titration (see the Supporting Information). A sample of P4−P6-wt-U107(pyr3) was annealed by heating to 90 °C in 10 mM Tris (pH 8.0) for 3 min followed by cooling to 25 °C before Mg^{2+} titration as usual. The overall intensity increase was slightly (∼10%) lower than for an unannealed sample, although the Mg^{2+} dependence was indistinguishable and all fluorescence components were clearly present. When the same annealing procedure was performed in 1× TB, the intensity increase was ∼40% lower in the annealed sample, although again the Mg^{2+} dependence was indistinguishable. Minor annealing effects on intensity (without changes in $[Mg^{2+}]_{1/2}$ values) were also observed with the pyr3-labeled double-stranded oligonucleotide.

A Shorter Tether to Pyrene Provides Similar Results. To determine the importance of the length of the tether connecting pyrene to the RNA, we examined pyr1-labeled RNA. The pyr1 chromophore has a tether from the 2′-amino to pyrene that is shorter by two carbon atoms compared with that of pyr3 (Figure 2A). P4−P6-wt-U107(pyr1) gave fluorescence components A and B similar to those of the

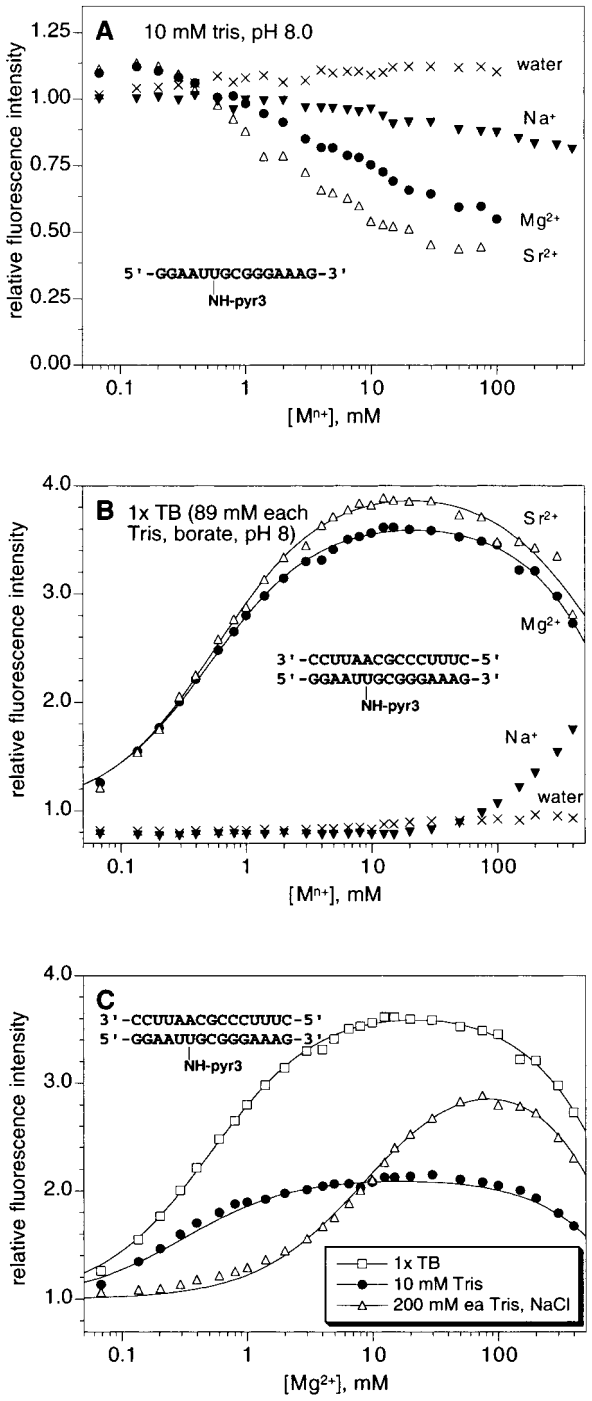

FIGURE 7: Equilibrium fluorescence titrations of a short RNA oligonucleotide labeled with pyrene. (A) Single-stranded 15-mer labeled with pyr3 (300 nM) in 10 mM Tris (pH 8.0), titrated with either Na^+, Mg^{2+}, or Sr^{2+}, or diluted with water. For the water dilution experiment, volumes of water equal to those of the appropriate metal ion stock solution for the other titrations were added; the data points were placed on the concentration axis along with the analogous metal ion data points. (B) Double-stranded 15-mer labeled with pyr3 (300 nM) in 1× TB, titrated as described for panel A. (C) Buffer dependence of the Mg^{2+} titration of double-stranded 15-mer labeled with pyr3. For all samples, relative fluorescence emission intensities at λ_{max} (380 ± 2 nm) were plotted. All data were fit to eq 4 of Materials and Methods with an I_{init} of 1.0 and n_A and n_B values of 1. In panel B, component A $[Mg^{2+}]_{1/2}$ = 0.51 ± 0.01 and component A $[Sr^{2+}]_{1/2}$ = 0.58 ± 0.03. In panel C, fit values of $[Mg^{2+}]_{1/2}$ were as follows: 10 mM Tris, 0.28 ± 0.03; 1× TB, 0.51 ± 0.01; and 200 mM Tris with 200 mM NaCl, 9.0 ± 0.7. Fit values of component B $[Mg^{2+}]$ (n_B = 1) were all >100 mM with very substantial error (>100%).

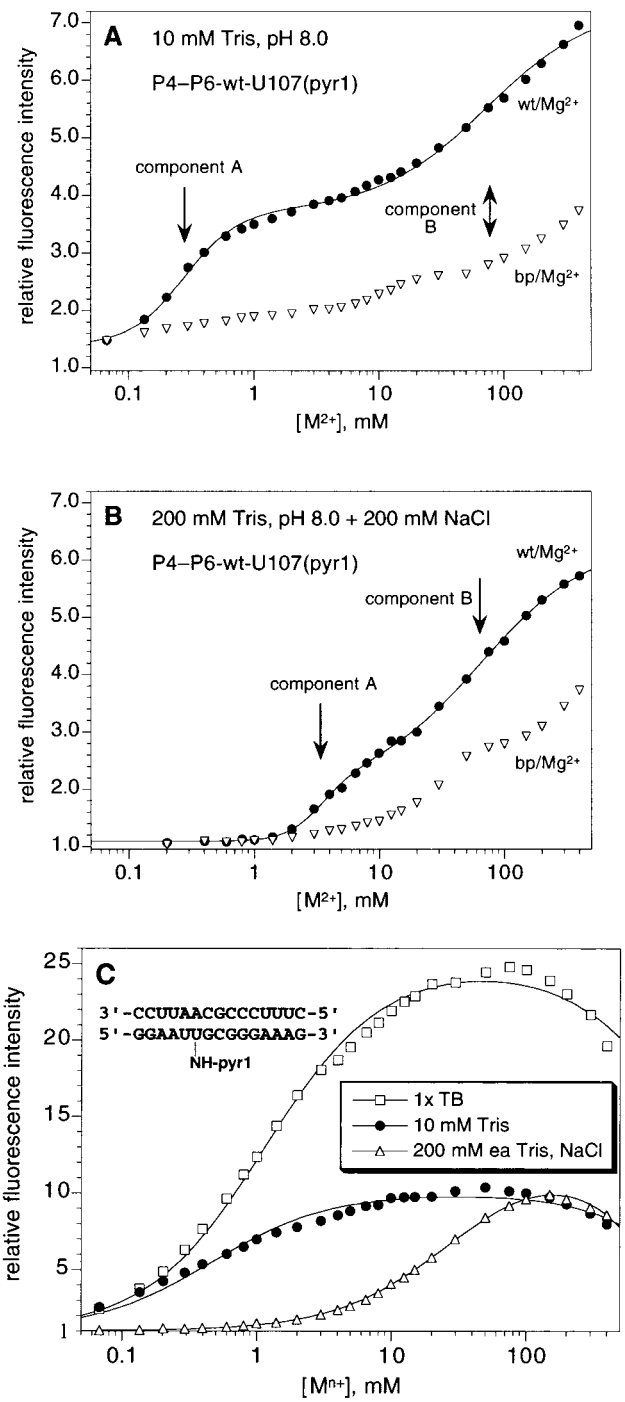

FIGURE 8: Equilibrium fluorescence titrations of RNA labeled with pyrene on a shorter tether (pyr1). (A) P4−P6-wt-U107(pyr1) in 10 mM Tris (pH 8.0). (B) P4−P6-wt-U107(pyr1) in 200 mM Tris (pH 8.0) with 200 mM NaCl. (C) Double-stranded 15-mer labeled with pyr1, titrated with Mg^{2+} in various buffers. Fit values of component A $[Mg^{2+}]_{1/2}$ (eq 4; I_{init} = 1.0, n_A = 1) were as follows: 10 mM Tris, 0.47 ± 0.05 mM; 1× TB, 1.2 ± 0.1 mM; and 200 mM Tris with 200 mM NaCl, 32 ± 1 mM. Fit values of component B $[Mg^{2+}]$ (n_B = 1) were all >100 mM with very substantial error (>100%).

pyr3 analogue, although the relative size of component B was larger (Figure 8A,B). The $[Mg^{2+}]_{1/2}$ values were similar to the analogous values for the pyr3 derivative (Table 1). In the highest-ionic strength buffer, a Mg^{2+} Hill coefficient n for component A of 2 was sufficient to fit the data (Figure 8B), whereas an n of 3 was required for the pyr3 data (Figure 5C). A double-stranded pyr1-labeled oligonucleotide exhibited markedly larger intensity changes relative to its pyr3

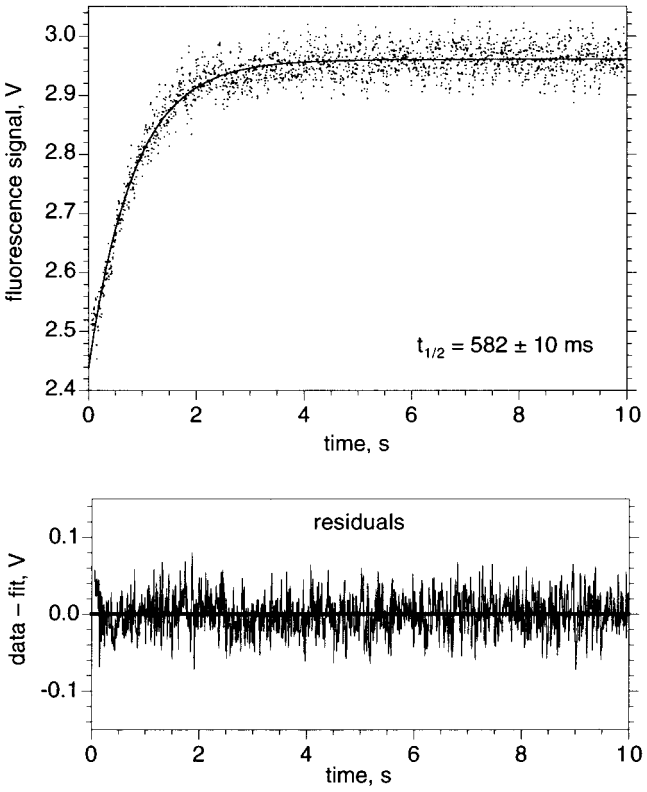

FIGURE 9: Stopped-flow kinetics experiment for monitoring tertiary folding of pyrene-labeled P4−P6. Final concentrations after mixing were 4 μM P4−P6-wt-U107(pyr3) and 0.7 mM Mg^{2+} in 1× TB at 25 °C. Data were acquired from 50 ms to 10 s after mixing of the RNA and Mg^{2+} samples (Applied Photosystems model 17MV stopped-flow apparatus, acquisition rate of 1 point/5 ms; instrument dead time of ~1.3 ms; λ_{exc} of 319 nm; Schott KV-370 emission filter). Four acquisitions were averaged and fit to a single-exponential equation. Residuals were calculated at each time point as data − fit; the random distribution of residuals around zero shows that the single-exponential equation adequately describes the data.

analogue (Figure 8C), while the Mg^{2+} dependence was shifted to slightly higher concentrations (compare Figure 8C with Figure 7C).

Initial Stopped-Flow Kinetic Analysis of P4−P6 Tertiary Folding. We have performed initial stopped-flow fluorescence experiments to examine the kinetics of P4−P6 tertiary folding induced by Mg^{2+}. The fluorescence of P4−P6-wt-U107(pyr3) in 1× TB at 25 °C was monitored immediately after mixing with an equal volume of Mg^{2+} in 1× TB, with a final Mg^{2+} concentration of 0.7 mM (Figure 9). This concentration is equal to the $[Mg^{2+}]_{1/2}$ for fluorescence component A in 1× TB but at least 1 order of magnitude lower than the $[Mg^{2+}]_{1/2}$ for component B (Table 1). Therefore, inasmuch as component A correlates with the level of P4−P6 tertiary folding, we expected the observed kinetics to reflect such folding. Indeed, under these conditions, a single kinetic component was cleanly resolved with a $t_{1/2}$ of 582 ± 10 ms; the $t_{1/2}$ decreased substantially at higher Mg^{2+} concentrations (data not shown). We tentatively assign the stopped-flow fluorescence transition of Figure 9 to P4−P6 tertiary folding. More comprehensive experiments are currently in progress.

DISCUSSION

New methods of monitoring RNA folding with fast time resolution are highly desirable. We report here a technique for monitoring RNA tertiary folding by fluorescence spectroscopy of RNA covalently labeled with the environmentally sensitive pyrene chromophore. Options for site-specific pyrene derivatization of RNA include substitution on any of the nucleotide bases (*44*−*47*), at an internal phosphate linkage (*48*−*50*), or on the ribose backbone at a 2′-hydroxyl position (*51*−*53*). However, for ease of synthesis, we chose to derivatize the P4−P6 RNA at a 2′-amino group, after first substituting a single 2′-hydroxyl. Pyrene was covalently and site-specifically attached via an amide linkage and short tether to the 2′-amino position of P4−P6 nucleotide U107, and the relative fluorescence intensity was monitored during titration with divalent ions that promote tertiary folding. This method allows us to follow both the equilibrium progress and real-time kinetics of the P4−P6 tertiary folding transition.

Pyrene Derivatization at U107 Is Relatively Nonperturbing to the RNA Structure. Nondenaturing gel experiments showed that substituting the U107 2′-hydroxyl group with 2′-amino and then covalently attaching the pyr3 or pyr1 chromophore does not greatly disrupt P4−P6 tertiary folding (Figure 3). The change in tertiary folding free energy ($\Delta\Delta G^{\circ\prime}$) of 0.5 kcal/mol due to U107(pyr3) or U107(pyr1) substitution was about equal to the effect of eliminating a single tertiary hydrogen bond in P4−P6 (*29*). Furthermore, the $\Delta\Delta G^{\circ\prime}$ due to U107(pyr3) was similar both in the context of P4−P6-wt (0.5 kcal/mol) and in the context of the P4−P6 U167C and G174A mutants (0.5−0.8 kcal/mol). Therefore, effects of the U107(pyr3) label are approximately additive with the effects of other structural changes on the tertiary folding free energy. Pyrene labeling may be generally useful for monitoring RNA tertiary folding, but it will be necessary to test in each case if appending the chromophore has any serious effect on the folding event that it is intended to monitor. Previous work has suggested that pyrene is nonperturbing to RNA structure (*26*).

Correlations between Biochemical and Fluorescence Experiments Demonstrate That Fluorescence Component A Is Due to Tertiary Folding. Our identification of fluorescence component A with P4−P6 tertiary folding was initially suggested by three observations. First, component A was present only for P4−P6 RNAs that can undergo tertiary folding. The unfolded control P4−P6-bp-U107(pyr3), which cannot physically fold, lacked component A in all the buffers that were tested (Figure 5). Second, component A in 1× TB buffer had about the same $[Mg^{2+}]_{1/2}$ of 0.7 mM (Figure 5B) as did the tertiary folding transition in nondenaturing gels (Figure 3). Third, component A was clearly cooperative with respect to Mg^{2+}, and P4−P6 folding is known to be cooperative (*29*, *30*). The component A Mg^{2+} Hill coefficient n_A was at least 3 in the higher-salt buffers, including 1× TB (Figure 5 and Table 1), consistent with an n of ≈4 for P4−P6 folding as determined by nondenaturing gel analysis in 1× TB (Figure 3).

Two sets of experiments showed more decisively that fluorescence component A is due to P4−P6 tertiary folding. The various divalent ions have differing abilities to promote either nondenaturing gel mobility changes or fluorescence component A, and the same trend of $Mg^{2+} \approx Ca^{2+} > Sr^{2+}$ was followed in both assays (compare Figures 3 and 5). In addition, remote mutations in P4−P6 that shifted the Mg^{2+} dependence of folding on nondenaturing gels also shifted

the fluorescence titration curves in a predictable way (Figure 6).

The molecular basis for each of these phenomena is partially understood. Divalent cation specificity of folding the entire *Tetrahymena* intron follows the trend $Mg^{2+} \geq Ca^{2+} > Sr^{2+}$ (*39*, *40*), similar to that observed here for folding of the P4−P6 domain. In the whole intron, this specificity was interpreted to reflect occupancy of specific structural sites that prefer different ionic radii or coordination geometries of the bound cations. The visualization of Mg^{2+} sites in the crystal structure of the P4−P6 domain, where some of the ions have ligands from multiple functional groups in a fixed geometry (*27*, *30*), has made it easier to understand why RNA folding exhibits metal ion specificity. On the other hand, suppression of destabilizing mutations by an increase in the Mg^{2+} ion concentration may have a more complex origin. Stabilizing interactions such as hydrogen bonding, base stacking, and metal ion coordination are counterbalanced by electrostatic repulsion of the two quasi-helical halves of P4−P6. Condensation of nonspecifically bound Mg^{2+} ions around the polyanionic backbone acts to relieve this repulsion and allow folding. Destabilization caused by site-specific mutations that remove favorable interactions or introduce steric clashes can be offset by increasing the solution Mg^{2+} concentration. This compensation may originate not in an increase in the number of nonspecifically bound Mg^{2+} ions, but rather because at higher bulk Mg^{2+} concentrations, the entropic penalty for concentrating Mg^{2+} around the RNA is lower (*54*). We note that the rescue of tertiary folding at high Mg^{2+} concentrations is not due to a generic charge-screening effect, for if this were the case, increasing Na^+ concentrations should recover folding, while the data in Figure 5 suggest that increasing Na^+ concentrations make tertiary folding *less* favorable.

Fluorescence Component B Is Likely Due to Local Reorganization. In contrast to fluorescence component A, component B was only a minor portion of the overall fluorescence change for labeled P4−P6 in lower-salt buffers. Component B also behaved in a manner very different from that of component A. In titrations of full-length P4−P6, component B was relatively insensitive to either divalent ion identity (Figure 5) or remote mutations that shifted the tertiary folding $[Mg^{2+}]_{1/2}$ on nondenaturing gels (Figure 6). For these reasons, we considered it unlikely that component B reflects large-scale P4−P6 tertiary folding. Another possibility is that component B is due to tertiary folding of the P5abc subdomain (Figure 1A), which occurs even in P4−P6-bp (*32*). This is implausible because the U167C and G174A mutations that significantly disrupt P5abc folding had little effect on the $[Mg^{2+}]_{1/2}$ of component B (Table 1), and in any case, P5abc is known to fold at a Mg^{2+} concentration *lower* than that required to fold the rest of P4−P6 (*32*). Because tertiary structure formation does not appear to be responsible for component B, we attribute this component of the fluorescence change to local reorganization of the RNA structure.

As models for such local changes, single- and double-stranded pyrene-labeled oligonucleotides were examined (Figures 7 and 8C). Of course, the rearrangements available to such oligonucleotides cannot model all the possible local changes in a more complex larger RNA. Nevertheless, the results suggest the type of fluorescence changes that can occur in nucleic acids lacking tertiary structure. The single-stranded pyr3-labeled oligonucleotide exhibited a largely nonspecific *decrease* in fluorescence with both monovalent and divalent ions (Figure 7A). Since all fluorescence changes observed with P4−P6 constructs were increases, the observations on the single-stranded oligonucleotide are of doubtful relevance. However, the double-stranded pyr3-labeled oligonucleotide exhibited an intensity increase at very high Na^+ concentrations (Figure 7B), which may reflect RNA structural changes induced by monovalent ions (*55*) or changes in chromophore−RNA interactions. With divalent ions, the double-stranded oligonucleotide also exhibited a significant rise in fluorescence that, like component B, was both essentially independent of divalent ion identity (Figure 7B) and noncooperative with respect to Mg^{2+} concentration (all titrations fit well with Hill coefficients n of 1). These results show that divalent ions can cause significant fluorescence changes even in pyrene-labeled oligonucleotides without tertiary structure, consistent with the proposal that fluorescence component B of P4−P6 is due to local structural reorganization.

Possible Physical Explanations for the Fluorescence Changes with Mg^{2+}. A potential conceptual drawback to some fluorescence experiments is that changes in fluorescence intensity can be difficult to explain in terms of atomic-level changes in the system being examined. That is, fluorescence changes may correlate with folding events, but precise physical explanations for these changes are usually unknown. In the study presented here, as P4−P6 folds after addition of Mg^{2+}, the relative fluorescence intensity (component A) is observed to increase substantially. At least two physical effects may contribute to this increase. (1) In the folded state, the pyrene chromophore may physically associate with the RNA more intimately than in the unfolded state; such interactions would be consistent with the observed fluorescence increase upon tertiary folding, because pyrene's fluorescence should be quenched more in aqueous surroundings than in the environment provided by RNA. (2) In the unfolded state, the pyrene chromophore may be close to pyrimidine bases, which are known to quench pyrene by an electron-transfer mechanism (*56*, *57*); folding could remove the chromophore from the vicinity of the quenching base, allowing the fluorescence to increase (*26*). Either or both of these effects may explain the observed fluorescence increase upon tertiary folding.

For reasons that are not yet understood, the pyrene-labeled oligonucleotides were more sensitive to environment than labeled full-length P4−P6. This was true both for pyr3-labeled RNA (compare Figures 5 and 7C) and especially for pyr1-labeled RNA (compare panels A and B of Figure 8 with panel C of Figure 8). Others have noted that small polypeptides do not correctly model side chain accessibilities in larger proteins (*58*). Because fluorescence intensity can correlate with chromophore accessibility [physical effect (1) in the previous paragraph], similar differences between oligonucleotides and large RNA molecules may contribute to our findings.

Conclusions and Outlook. Our experiments validate the use of a single, internally tethered fluorescent chromophore in monitoring P4−P6 tertiary folding, and we hope that this method will be generally useful for following the tertiary folding of large RNAs. Several points must be considered

in applying such methods to other systems. First, the usefulness of any given chromophore almost certainly depends on the particular site of substitution. The availability of the P4−P6 crystal structure was a significant advantage in choosing an appropriate site for pyrene labeling; in systems for which such high-resolution structural data are not yet available, the proportion of sites that can be successfully derivatized remains to be determined. Second, we have shown that the length of the tether to the chromophore affects the observed fluorescence, and it is likely that the optimum tether length will depend strongly on the particular site of labeling. Third, the choice of buffer can significantly affect the observations. For instance, in the P4−P6 system, fluorescence component A corresponding to tertiary folding is both more clearly resolved and a greater proportion of the overall signal in buffers with relatively low ionic strengths. Finally, some chromophores may be useful in cases where others are not, and probes other than pyrene should be tested in similar experiments.

By using circular permutation (*59*) to bring various nucleotides close to the 5′- or 3′-end to allow splint ligation, many large RNAs should be amenable to the fluorescence technique reported here. We are also continuing stopped-flow experiments such as those whose results are depicted in Figure 9 to determine real-time P4−P6 folding kinetics. Using pyrene-labeled oligonucleotides, we have been able to resolve kinetic events with $t_{1/2}$ values of ∼1 ms (data not shown), so fluorescence holds much promise for resolution of RNA tertiary folding on the millisecond time scale.

ACKNOWLEDGMENT

We thank Susy Kohout and Eric Nalefski for invaluable guidance on fluorescence spectroscopy and for essential discussions, Scott Cohen for discussions on initial experimental design, members of the Cech lab for helpful comments, Doug Turner, Phil Bevilacqua, Jamie Williamson, Martha Rook, and Nils Walter for conversations on fluorescently labeled RNA, Stephen Scaringe (Dharmacon Research), Jeff Pleiss, and Leo Beigelman (Ribozyme Pharmaceuticals) for discussions on RNA oligonucleotide synthesis and derivatization, Stephen Scaringe for ongoing collaborative efforts to prepare modified RNA oligonucleotides and for HPLC analysis of the pyrene-labeled 15-mer, and Anne Gooding for providing T7 RNA polymerase. We are grateful to Eric Nalefski for comments on the manuscript and to Daniel Harrington for assistance in preparing Figure 1B.

SUPPORTING INFORMATION AVAILABLE

Optimization of the pyrene derivatization reaction, determination of the free 2′-amino content of the pyr3-labeled oligonucleotide by treatment with a reactive NHS ester, titration of labeled P4−P6-wt with Na^+ in 10 mM Tris and with Mg^{2+} in other buffers, and determination of annealing effects on the Mg^{2+} titrations of labeled P4−P6-wt and the labeled oligonucleotide duplex. This material is available free of charge via the Internet at http://pubs.acs.org.

NOTE ADDED IN PROOF

The manuscript cited as Silverman et al., manuscript submitted for publication, is now in press in *RNA*.

REFERENCES

1. Banerjee, A. R., and Turner, D. H. (1995) *Biochemistry 34*, 6504−6512.
2. Zarrinkar, P. P., and Williamson, J. R. (1994) *Science 265*, 918−924.
3. Zarrinkar, P. P., Wang, J., and Williamson, J. R. (1996) *RNA 2*, 564−573.
4. Treiber, D. K., Rook, M. S., Zarrinkar, P. P., and Williamson, J. R. (1998) *Science 279*, 1943−1946.
5. Downs, W. D., and Cech, T. R. (1996) *RNA 2*, 718−732.
6. Sclavi, B., Sullivan, M., Chance, M. R., Brenowitz, M., and Woodson, S. A. (1998) *Science 279*, 1940−1943.
7. Cole, P. E., and Crothers, D. M. (1972) *Biochemistry 11*, 4368−4374.
8. Maglott, E. J., and Glick, G. D. (1997) *Nucleic Acids Res. 25*, 3297−3301.
9. Maglott, E. J., Deo, S. S., Przykorska, A., and Glick, G. D. (1998) *Biochemistry 37*, 16349−16359.
10. Eftink, M. R. (1994) *Biophys. J. 66*, 482−501.
11. Chen, Y., and Barkley, M. D. (1998) *Biochemistry 37*, 9976−9982.
12. Eftink, M. (1997) *Methods Enzymol. 278*, 221−257.
13. Tuschl, T., Gohlke, C., Jovin, T. M., Westhof, E., and Eckstein, F. (1994) *Science 266*, 785−789.
14. Bassi, G. S., Murchie, A. I. H., Walter, F., Clegg, R. M., and Lilley, D. M. J. (1997) *EMBO J. 16*, 7481−7489.
15. Perkins, T. A., Wolf, D. E., and Goodchild, J. (1996) *Biochemistry 35*, 16370−16377.
16. Walter, N. G., Hampel, K. J., Brown, K. M., and Burke, J. M. (1998) *EMBO J. 17*, 2378−2391.
17. Walter, N. G., Burke, J. M., and Millar, D. P. (1999) *Nat. Struct. Biol. 6*, 544−549.
18. Turner, D. H., Li, Y., Fountain, M., Profenno, L., and Bevilacqua, P. C. (1996) in *Nucleic Acids in Molecular Biology* (Eckstein, F., and Lilley, D. M. J., Eds.) Vol. 10, pp 19−32, Springer-Verlag, Berlin.
19. Bevilacqua, P. C., Kierzek, R., Johnson, K. A., and Turner, D. H. (1992) *Science 258*, 1355−1358.
20. Bevilacqua, P. C., Sugimoto, N., and Turner, D. H. (1996) *Biochemistry 35*, 648−658.
21. Walter, N. G., and Burke, J. M. (1997) *RNA 3*, 392−404.
22. Pieken, W. A., Olsen, D. B., Benseler, F., Aurup, H., and Eckstein, F. (1991) *Science 253*, 314−317.
23. Heidenreich, O., Pieken, W., and Eckstein, F. (1993) *FASEB J. 7*, 90−96.
24. Heidenreich, O., Benseler, F., Fahrenholz, A., and Eckstein, F. (1994) *J. Biol. Chem. 269*, 2131−2138.
25. Qin, P. Z., and Pyle, A. M. (1997) *Biochemistry 36*, 4718−4730.
26. Kierzek, R., Li, Y., Turner, D. H., and Bevilacqua, P. C. (1993) *J. Am. Chem. Soc. 115*, 4985−4992.
27. Cate, J. H., Gooding, A. R., Podell, E., Zhou, K., Golden, B. L., Kundrot, C. E., Cech, T. R., and Doudna, J. A. (1996) *Science 273*, 1678−1685.
28. Laggerbauer, B., Murphy, F. L., and Cech, T. R. (1994) *EMBO J. 13*, 2669−2676.
29. Silverman, S. K., and Cech, T. R. (1999) *Biochemistry 38*, 8691−8702.
30. Cate, J. H., Hanna, R. L., and Doudna, J. A. (1997) *Nat. Struct. Biol. 4*, 553−558.
31. Grosshans, C. A., and Cech, T. R. (1991) *Nucleic Acids Res. 19*, 3875−3880.
32. Murphy, F. L., and Cech, T. R. (1993) *Biochemistry 32*, 5291−5300.
33. Sigurdsson, S. T., and Eckstein, F. (1996) *Nucleic Acids Res. 24*, 3129−3133.
34. Cohen, S. B., and Cech, T. R. (1997) *J. Am. Chem. Soc. 119*, 6259−6268.
35. Hendrix, C., Devreese, B., Rozenski, J., Van Aerschot, A., De Bruyn, A., Van Beeumen, J., and Herdewijn, P. (1995) *Nucleic Acids Res. 23*, 51−57.
36. Matulic-Adamic, J., Beigelman, L., Dudycz, L. W., Gonzalez, C., and Usman, N. (1995) *Bioorg. Med. Chem. Lett. 5*, 2721−2724.

37. Moore, M. J., and Sharp, P. A. (1992) *Science 256*, 992−997.
38. Murphy, F. L., and Cech, T. R. (1994) *J. Mol. Biol. 236*, 49−63.
39. Celander, D. W., and Cech, T. R. (1991) *Science 251*, 401−407.
40. Grosshans, C. A., and Cech, T. R. (1989) *Biochemistry 28*, 6888−6894.
41. Szewczak, A. A., and Cech, T. R. (1997) *RNA 3*, 838−849.
42. Uhlenbeck, O. C. (1995) *RNA 1*, 4−6.
43. Walstrum, S. A., and Uhlenbeck, O. C. (1990) *Biochemistry 29*, 10573−10576.
44. Lee, H., Hinz, M., Stezowski, J. J., and Harvey, R. G. (1990) *Tetrahedron Lett. 31*, 6773−6776.
45. Telser, J., Cruickshank, K. A., Morrison, L. E., and Netzel, T. L. (1989) *J. Am. Chem. Soc. 111*, 6966−6976.
46. Roget, A., Bazin, H., and Teoule, R. (1989) *Nucleic Acids Res. 17*, 7643−7651.
47. Allerson, C. R., Chen, S. L., and Verdine, G. L. (1997) *J. Am. Chem. Soc. 119*, 7423−7433.
48. Fidanza, J. A., and McLaughlin, L. W. (1992) *J. Org. Chem. 57*, 2340−2346.
49. Ozaki, H., and McLaughlin, L. W. (1992) *Nucleic Acids Res. 20*, 5205−5214.
50. Musier-Forsyth, K., and Schimmel, P. (1994) *Biochemistry 33*, 773−779.
51. Manoharan, M., Guinosso, C. J., and Cook, P. D. (1991) *Tetrahedron Lett. 32*, 7171−7174.
52. Yamana, K., Ohashi, Y., Nunota, K., Kitamura, M., Nakano, H., Sangen, O., and Shimidzu, T. (1991) *Tetrahedron Lett. 32*, 6347−6350.
53. Yamana, K., Aota, R., and Nakano, H. (1995) *Tetrahedron Lett. 36*, 8427−8430.
54. Manning, G. S. (1978) *Q. Rev. Biophys. 11*, 179−246.
55. Cole, P. E., Yang, S. K., and Crothers, D. M. (1972) *Biochemistry 11*, 4358−4368.
56. Manoharan, M., Tivel, K. L., Zhao, M., Nafisi, K., and Netzel, T. L. (1995) *J. Phys. Chem. 99*, 17461−17472.
57. Netzel, T. L., Zhao, M., Nafisi, K., Headrick, J., Sigman, M. S., and Eaton, B. E. (1995) *J. Am. Chem. Soc. 117*, 9119−9128.
58. Creamer, T. P., Srinivasan, R., and Rose, G. D. (1995) *Biochemistry 34*, 16245−16250.
59. Pan, T., and Uhlenbeck, O. C. (1993) *Gene 125*, 111−114.

BI991333F